The Canadian Mineralogist
Vol. 60, pp. 775-786 (2022)
DOI: 10.3749/canmin.2200005

MASS BIAS CORRECTIONS FOR HYDROGEN AND OXYGEN ISOTOPE ANALYSIS OF TOURMALINE BY SECONDARY ION MASS SPECTROMETRY

Jessica WHATTAM, Ryan SHARPE[§], Steph SKELTON, Maxwell C. DAY, Mostafa FAYEK, and Frank C. HAWTHORNE

Department of Earth Sciences, 240 Wallace Building, The University of Manitoba, 125 Dysart Road, Winnipeg, R3T 2N2, Canada

Abstract

Hydrogen (δ^2H) and oxygen ($\delta^{18}O$) stable isotopes are used to trace fluid sources, metals, and contaminants in the environment and Earth's subsurface. Tourmaline-supergroup minerals provide an opportunity to quantify both δ^2H and $\delta^{18}O$ from the same grain using *in situ* analytical techniques (*e.g.*, Secondary Ion Mass Spectrometry – SIMS). These minerals occur in a wide variety of geological environments and have a wide range of chemical compositions. However, large differences in chemical composition are problematic during SIMS analysis, as instrumental mass fractionation (IMF) often varies with the chemical composition of the mineral. Therefore, calibration models derived by analyzing tourmalines of different chemical composition must be developed for accurate analysis by SIMS. Hydrogen and oxygen isotope analysis was done on six reference tourmaline samples using a CAMECA 7f SIMS instrument operating at extreme energy filtering. Spot-to-spot repeatability for tourmalines was in the range 4–5‰ and 0.6–1.0‰ for δ^2H and $\delta^{18}O$, respectively. There is a strong correlation between IMF and several elements (B, Si, Ca, Fe, and Fe#). Iron content is the most robust predictor of IMF, and we report two calibration curves for the correction of δ^2H and $\delta^{18}O$ measured by SIMS using reference tourmaline crystals with different Fe contents, ranging from 0.00 to 14.00 wt.% Fe. This is the first calibration curve used to correct for the fractionation of hydrogen isotope ratios in tourmaline as measured by SIMS. Tourmaline-supergroup minerals require a suite of at least three, with a range of Fe content, to ensure accurate and precise H and O analysis by SIMS. Crystallographic orientation effects were not observed for these tourmalines.

Keywords: SIMS, oxygen, hydrogen, tourmaline, IMF.

Introduction

Tourmaline-supergroup minerals have a complicated mineral structure, include a very wide range of chemical compositions, and can exhibit complex zoning (Hawthorne & Dirlam 2011). These minerals occur in a wide range of geological environments and are stable over a wide range of temperature and pressure conditions. Thus, they are well suited for studies that utilize chemical and isotope indicators. Stable isotopes of hydrogen ($^2H/^1H$) and oxygen ($^{18}O/^{16}O$) of tourmaline have been used to establish formation processes for critical metal deposits (Kotzer & Kyser 1995, Hawthorne & Dirlam 2011, Reid *et al*. 2013), to trace mineralizing and alteration fluids (Marger *et al*. 2019), and to estimate temperature conditions (Valley 2001).

Secondary ion mass spectrometry (SIMS) is well suited for the study of tourmaline isotope geochemistry because the technique has straightforward sample preparation, is minimally destructive, and allows analysis of different mineral generations and zoned minerals on a micron scale. This is particularly significant for tourmaline, which often has complex zonation patterns and may occur as trace accessory minerals in various rock types (Hawthorne & Dirlam 2011). During SIMS analysis, instrumental mass fractionation (IMF) occurs due to a variety of processes including secondary atom ionization (sputtering) and extraction (Sigmund 1969, Shroeer *et al*. 1973), secondary ion transmission (Shimizu & Hart

§ *Corresponding author e-mail address*: Ryan.Sharpe@umanitoba.ca

1982), and detection (Lyon *et al*. 1994). Fractionation is also dependent on the chemical composition of the sample (matrix effects) and crystallography (crystallographic orientation effects), which can be significant for some minerals (*e.g*., sphalerite, magnetite; Kozdon *et al*. 2010, Huberty *et al*. 2010). Both instrumental fractionation and matrix effects can be corrected using reference materials (RM) that are compositionally similar to the unknowns (Adams *et al*. 1989, Hervig *et al*. 1992, Riciputi *et al*. 1998). Below, we define mass bias as the combination of IMF and matrix effects.

Two previous SIMS studies have been conducted on tourmaline, measuring $\delta^{18}O$ (Marger *et al*. 2019) and $\delta^{11}B$ (Marger *et al*. 2020). Both studies utilized a CAMECA IMS 1280HR large radius magnetic-sector SIMS instrument and used mass resolving power (MRP) to resolve interferences. For $\delta^{18}O$, IMF varied from 0.10 to 2.15‰ and was observed to be a linear function of Fe (*apfu*) and Al_{tot} (*apfu*). For $\delta^{11}B$, IMF was more variable and ranged from –0.17 to 7.49‰. Calibration was more complex for boron isotopes and a multiple linear, error-weighted least square regression was fitted using three chemical parameters (FeO + MnO, SiO_2, and F). No crystallographic orientation effects were observed for either isotope system.

The Fe content of tourmaline-supergroup minerals may range from 0 wt.% (*e.g.,* dravite; ^{Y}[Fe / (Fe + Mg)] $\leq$ 0.5) to more than 15 wt.% (*e.g.,* schorl; ^{Y}[Fe / (Fe + Mg)] $\geq$ 0.5; Henry *et al*. 2011). Most SIMS studies of minerals with variable chemical composition correct for matrix effects through discovery and application of systematic relationships with one or more chemical components. Reference material representing a range of chemical compositions and independently known isotopic compositions are analyzed and used to correct for IMF during the same session as unknown sample analysis (Ickert & Stern 2013, Othmane *et al*. 2015, Śliwiński *et al*. 2016, Marger *et al*. 2019). Here we use six tourmaline RMs with different chemical compositions to develop calibration curves for hydrogen and oxygen isotope analysis by SIMS and to evaluate crystallographic orientation effects.

Sample Preparation

Six tourmaline RMs from the mineral collection at the University of Manitoba were studied: BT01, BT02, DRG01, GE01, PE01, and PE02. All RMs except PE02 were used to develop calibration curves, and PE02 and BT01 were used to evaluate orientation effects. Tourmalines were mounted into 25 mm diameter pucks using Buehler Epo-Thin epoxy and left to cure for ~24 h. The mounts were polished using a Struers LaboPol-20 polishing machine with a LaboForce-50 specimen mover, starting with 320-grit sandpaper and finishing with 1 μm diamond polishing compound. Tourmalines are hard (H ~ 7) and can be difficult to polish. Over-polishing can result in high relief of grains and introduce randomness to IMF (Kita *et al*. 2009). Samples were examined with a white light microscope to check for mount relief. Prior to analysis, mounts were cleaned in an ultrasonic cleaner, first using tap water, then distilled water, and finally ethanol. To evaluate crystal orientation effects, PE02 and BT01 were cut and mounted both perpendicular and parallel to their **c**-axes.

Experimental Methods

Electron probe microanalysis

Chemical compositions of samples were measured by electron probe microanalysis at the University of Manitoba using a CAMECA SX-100 electron microprobe operating in wavelength dispersive mode with a voltage of 15 kV, a beam current of 20 nA, and beam size of 10 μm. The following standards were used for *K*α lines: Na, albite; Si, Fe, fayalite; Ca, diopside; F, topaz; Mg, forsterite; Al, andalusite; K, orthoclase; Ti, titanite; Mn, spessartine. A total of 15–20 analytical points were measured on each sample and data were corrected using the PAP procedure from Pouchou & Pichoir (1985). Mean element concentrations (wt.%) are given in Table 1. Mean oxide concentrations (wt.%) are given in Table 2 along with unit formulae calculated on the basis of (O^{2-}, OH^-, F) = 31 atoms per formula unit (*apfu*) with ^{V}(OH) = 3 *apfu* and ^{W}(O^{2-}, OH^-, F^-) = 1 *apfu*. B_2O_3 was calculated using the WinTcac 2014 software assuming stoichiometric B^{3+} (B^{3+} = 3 *apfu*). Li_2O and H_2O were calculated using procedures and assumptions described by Yavuz *et al*. (2014) and Henry & Dutrow *et al*. (1996). All tourmalines were classified and named following Henry *et al*. (2011; Table 2).

Bulk isotope composition

Bulk hydrogen isotope values were measured using continuous-flow isotope-ratio mass spectrometry (Clayton & Mayeda 1963) at the University of Manitoba. Samples were weighed into silver capsules (approximately 2–3 mg), degassed for 1 h at 100 °C, and then crushed and subsequently loaded into a zero-blank auto sampler. The hydrogen isotopic composition was measured using a Thermo-Finnigan thermocombustion elemental analyzer (TC/EA) coupled to a Thermo-Finnigan Delta^{Plus} XP continuous-flow isotope-ratio mass spectrometer (CF-IRMS). The δ^2H values are reported using delta (δ) notation in permil (‰) relative to Vienna Standard Mean Ocean Water

TABLE 1. MAJOR-ELEMENT CONCENTRATIONS OF THE SIX TOURMALINE RM

	BT01	1SD	BT02	1SD	PE01	1SD	PE02	1SD	GE01	1SD	DRG01	1SD
B	3.13	-	3.26	-	3.39	-	3.36	-	3.35	-	3.32	-
Si	16.00	0.17	16.72	0.18	17.62	0.18	17.48	0.18	17.17	0.18	16.96	0.18
Al	16.46	0.18	18.34	0.19	23.06	0.21	22.38	0.21	16.36	0.18	17.47	0.18
Mg	0.16	0.02	1.01	0.05	b.d.	-	b.d.	-	7.83	0.12	5.13	0.10
Ti	0.29	0.02	0.07	0.01	b.d.	-	b.d.	-	0.31	0.02	0.17	0.02
Mn	0.06	0.04	0.46	0.06	b.d.	-	0.52	0.06	b.d.	-	b.d.	-
Fe^{2+}	14.00	0.26	9.86	0.21	b.d.	-	b.d.	-	b.d.	-	3.80	0.14
Fe^{3+}	-	-	-	-	-	-	-	-	-	-	-	-
Ca	0.01	0.01	0.09	0.01	b.d.	-	0.61	0.03	1.55	0.04	0.46	0.02
Na	1.84	0.06	1.07	0.04	1.45	0.05	1.38	0.05	1.45	0.05	1.50	0.05
K	0.04	0.01	b.d.	-	b.d.	-	b.d.	-	b.d.	-	b.d.	-
Li	0.03	-	0.04	-	0.63	-	0.67	-	0.05	-	0.02	-
F	1.36	-	0.16	-	0.93	-	1.44	-	1.11	-	0.73	-
H	0.30	-	0.34	-	0.35	-	0.32	-	0.35	-	0.35	-

b.d.: below detection limit of the electron microprobe
All data reported in element weight percent

(VSMOW). The precision of the measurements, based on duplicate sample analyses, is 2–6‰ (1SD). The accuracy of sample analyses, based on primary/secondary standards, is 3‰ (1SD).

Bulk oxygen isotope values were obtained using the BrF_5 method at Queen's University. Oxygen was extracted from 5 mg samples at 550–600 °C according to the conventional BrF_5 procedure of Clayton & Mayeda (1963) and analyzed on a Thermo-Finnigan Delta^{Plus} XP CF-IRMS. The $\delta^{18}O$ values are also reported using the delta (δ) notation in units of permil (‰) relative to VSMOW international standard. Precision and accuracy of sample analyses were both <0.1‰ (1SD). Precision is based upon duplicate sample analyses and accuracy is based upon primary/secondary standard analyses.

Secondary ion mass spectrometer analysis

Hydrogen isotope analysis was done with a CAMECA 7f magnetic-sector SIMS instrument at the University of Manitoba between June 10th, 2015, and September 25th, 2020. The analytical protocol was modified from Liu *et al*. (2011). Prior to analysis the

TABLE 2. CHEMICAL COMPOSITION (wt.%), UNIT FORMULA (*apfu*), AND CLASSIFICATION OF TOURMALINE RM

	BT01	1SD	BT02	1SD	PE01	1SD	PE02	1SD	GE01	1SD	DRG01	1SD
wt.%												
B_2O_3*	10.09	-	10.51	-	10.95	-	10.84	-	10.82	-	10.70	-
SiO_2	34.24	0.36	35.78	0.37	37.70	0.38	37.40	0.38	36.74	0.38	36.29	0.38
Al_2O_3	31.11	0.34	34.65	0.36	43.58	0.40	42.28	0.40	30.91	0.34	33.01	0.34
MgO	0.26	0.03	1.68	0.08	b.d.	-	b.d.	-	12.99	0.20	8.51	0.16
TiO_2	0.48	0.03	0.11	0.02	b.d.	-	b.d.	-	0.51	0.03	0.29	0.03
MnO	0.08	0.05	0.60	0.08	b.d.	-	0.67	0.08	b.d.	-	b.d.	-
FeO	18.02	0.33	12.69	0.27	b.d.	-	b.d.	-	b.d.	-	4.89	0.18
Fe_2O_3*	-	-	-	-	-	-	-	-	-	-	-	-
CaO	0.02	0.01	0.12	0.01	b.d.	-	0.85	0.04	2.17	0.05	0.65	0.03
Na_2O	2.48	0.08	1.44	0.05	1.96	0.07	1.86	0.07	1.96	0.07	2.03	0.07
K_2O	0.05	0.01	b.d.	-	b.d.	-	b.d.	-	b.d.	-	b.d.	-
Li_2O*	0.06	-	0.09	-	1.35	-	1.44	-	0.11	-	0.04	-
F	1.36	-	0.16	-	0.93	-	1.44	-	1.11	-	0.73	-
H_2O*	2.66	-	3.03	-	3.09	-	2.87	-	3.13	-	3.09	-
O=F	−0.57	-	−0.07	-	−0.39	-	−0.61	-	−0.47	-	−0.31	-
Total	100.34		100.79		99.17		99.04		99.98		99.92	

TABLE 2. CONTINUED.

	BT01	1SD	BT02	1SD	PE01	1SD	PE02	1SD	GE01	1SD	DRG01	1SD
Formula (*apfu*)												
B^{3+}	3.00		3.00		3.00		3.00		3.00		3.00	
ΣB	**3.00**		**3.00**		**3.00**		**3.00**		**3.00**		**3.00**	
Si^{4+}	5.90		5.92		5.98		6.00		5.90		5.89	
Al^{3+}	0.10		0.08		0.02		0.00		0.10		0.11	
ΣT	**6.00**		**6.00**		**6.00**		**6.00**		**6.00**		**6.00**	
Al^{3+}	6.00		6.00		6.00		6.00		5.76		6.00	
Fe^{3+}	0.00		0.00		0.00		0.00		0.00		0.00	
Mg^{2+}	0.00		0.00		0.00		0.00		0.24		0.00	
ΣZ	**6.00**		**6.00**		**6.00**		**6.00**		**6.00**		**6.00**	
Al^{3+}	0.22		0.67		2.14		1.98		0.00		0.22	
Fe^{2+}	2.60		1.76		0.00		0.00		0.00		0.66	
Mn^{2+}	0.01		0.08		0.00		0.09		0.00		0.00	
Ti^{4+}	0.06		0.01		0.00		0.00		0.06		0.04	
Mg^{2+}	0.07		0.41		0.00		0.00		2.87		2.06	
Li^{+}	0.05		0.06		0.86		0.93		0.07		0.02	
ΣY	**3.01**		**2.99**		**3.00**		**3.00**		**3.00**		**3.00**	
Na^{+}	0.83		0.46		0.60		0.58		0.61		0.64	
K^{+}	0.01		0.00		0.00		0.00		0.00		0.00	
Ca^{2+}	0.00		0.02		0.00		0.15		0.37		0.11	
vacancy	0.16		0.52		0.40		0.28		0.02		0.25	
ΣX	**1.00**		**1.00**		**1.00**		**1.01**		**1.00**		**1.00**	
OH^{-}	3.00		3.00		3.00		3.00		3.00		3.00	
O^{2-}	0.00		0.00		0.00		0.00		0.00		0.00	
ΣV	**3.00**		**3.00**		**3.00**		**3.00**		**3.00**		**3.00**	
OH^{-}	0.06		0.34		0.27		0.07		0.35		0.35	
O^{2-}	0.20		0.58		0.26		0.20		0.09		0.27	
F^{-}	0.74		0.08		0.47		0.73		0.56		0.38	
ΣW	**1.00**		**1.00**		**1.00**		**1.00**		**1.00**		**1.00**	
Group	Alkali		X-vacant		Alkali		Alkali		Alkali		Alkali	
Species series (W-site)	Fluor-		Oxy-		Fluor-		Fluor-		Fluor-		Fluor-	
Subgroup	1		3		2		2		1		1	
Name	Fluor-schorl		Oxy-foitite		Fluor-elbaite		Fluor-elbaite		Fluor-dravite		Fluor-dravite	

B_2O_3* calculated using WinTcac software assuming stoichiometric B_2O_3 (B = 3 *apfu*).
Li_2O*, H_2O*, and O^{2-} calculated using procedures and assumptions outlined by Yavuz *et al.* (2014) and Henry & Dutrow (1996).
b.d.: below detection limit.
Classification from Henry *et al.* (2011).

mounts were sputtered-coated with a ~40 nm layer of gold to prevent charging. A liquid nitrogen trap was used to keep the vacuum levels $<5.0 \times 10^{-9}$ Torr. Analysis was done using a ~40 nA primary O^{-} ion beam, accelerated at 12.5 kV. The beam was focused to a 50 μm spot using a 750 μm aperture in the primary column. The largest available contrast and field apertures (400 and 1800 μm, respectively), in conjunction with a 150 μm image field and an energy band pass of ±25 eV, were used to maximize sensitivity. A sample accelerating voltage of +9.95 kV was used, with the electrostatic analyzer in the secondary column set to accept +10.00 kV. Entrance slits were set to 65.0 μm. A mass resolving power of 800 (measured at 10% valley) produced flat-top peaks and in combination with a 50-volt sample offset resolved the expected H_2^{+} interference (Liu *et al.* 2011). Two isotopes of hydrogen (^1H and ^2H) were

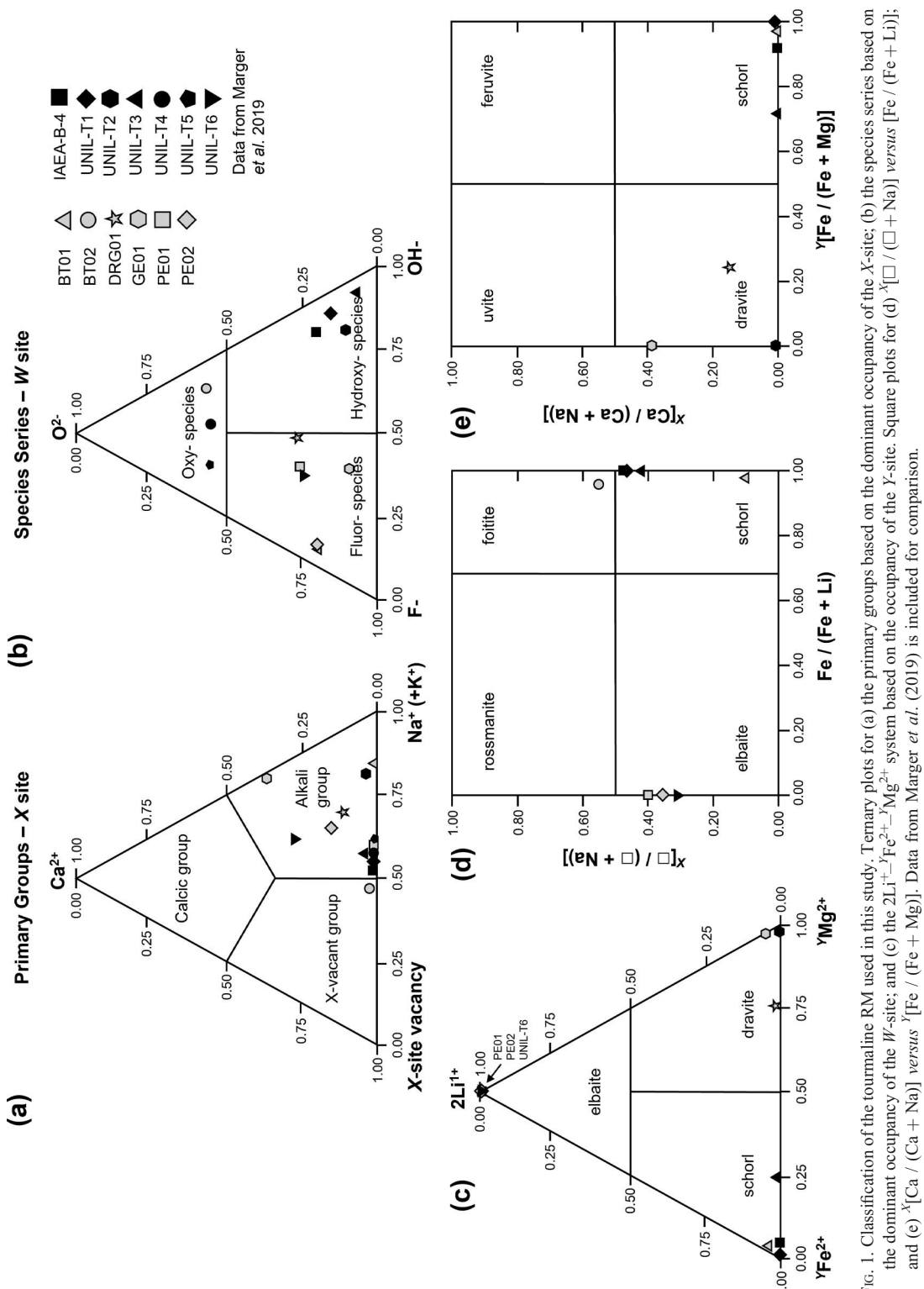

FIG. 1. Classification of the tourmaline RM used in this study. Ternary plots for (a) the primary groups based on the dominant occupancy of the *X*-site; (b) the species series based on the dominant occupancy of the *W*-site; and (c) the $2Li^{1+}$–$^{Y}Fe^{2+}$–$^{Y}Mg^{2+}$ system based on the occupancy of the *Y*-site. Square plots for (d) $^{X}[\square / (\square + Na)]$ *versus* [Fe / (Fe + Li)]; and (e) $^{X}[Ca / (Ca + Na)]$ *versus* ^{Y}[Fe / (Fe + Mg)]. Data from Marger *et al.* (2019) is included for comparison.

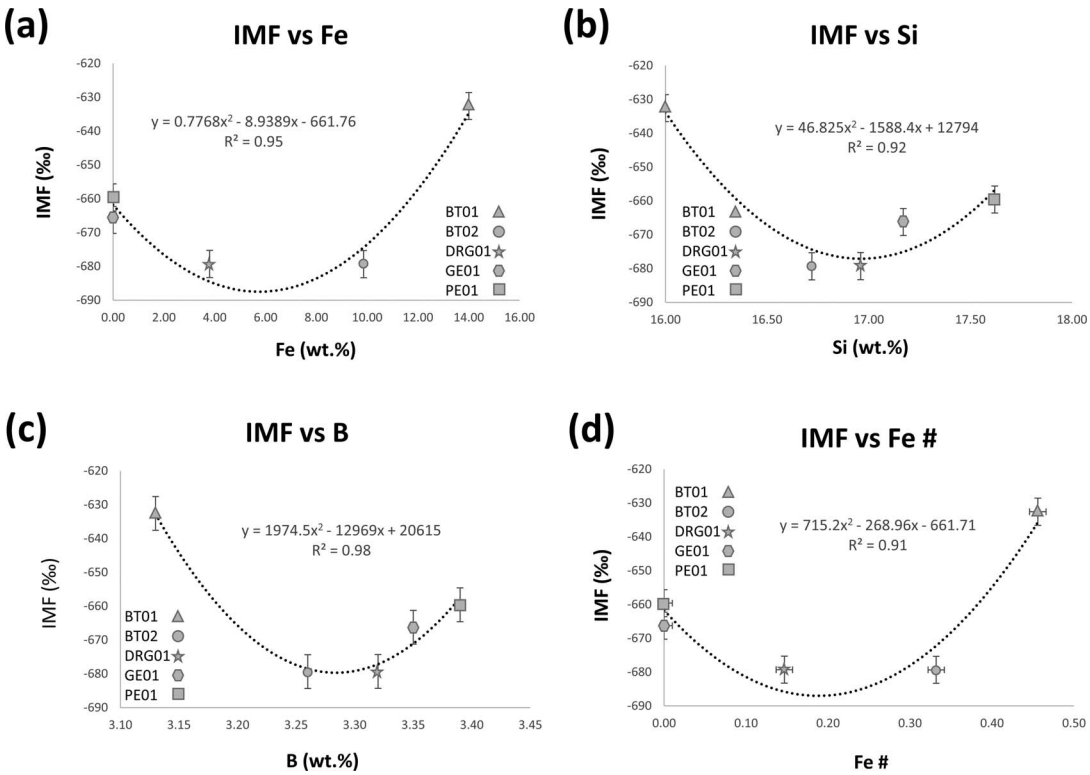

FIG. 2. Hydrogen IMF (‰) *versus* (a) Fe, (b) Si, (c) B, and (d) Fe #: Fe / (Fe + Mg + Al + Mn + Li) for the five tourmaline RM. The curves are defined by a 2nd order polynomial with an R^2 value of >0.91. Data is from the 2020 session; error bars not shown in the **x**-direction are collapsed into the size of the RM symbol.

measured by alternating the magnetic field between masses. Ions were detected using an electron multiplier. Analytical spots were pre-sputtered for 60 s and a typical analysis comprised 90 analytical cycles, in total lasting ~14 min. The within-spot repeatability for hydrogen was between 6 and 8‰ (1SD).

Oxygen isotope analysis occurred between August 26th, 2015, and September 17th, 2020, using the same SIMS instrument. The analytical protocol used is similar to that of Hervig *et al*. (1992). Analysis was done using a ~4 nA primary Cs^+ ion beam, accelerated at 10.0 kV. The beam was focused to a 15 μm spot using a 750 μm aperture in the primary column. An electron gun provided charge compensation. The largest available contrast and field apertures (400 and 1800 μm, respectively), in conjunction with a 150 μm image field and an energy bandpass of ±25 eV, were used to maximize sensitivity. The sample accelerating voltage was –9.7 kV, with the electrostatic analyzer in the secondary column set to accept –10.0 kV. This 300 V sample offset suppressed isobaric interferences. Entrance slits were set to 225 μm and a mass resolving power of 350 was used (measured at 10% valley), producing flat-top peaks. Two isotopes of oxygen (^{16}O and ^{18}O) were measured by alternating the magnetic field between masses; ions were detected using an electron multiplier. A typical analysis comprised 70 cycles and lasted ~10 min. The within-spot repeatability for oxygen is between 1.1 and 1.2‰ (1SD).

The fractionation factor (FF or αSIMS) was calculated for each analysis. Our procedure is similar to that of Riciputi *et al*. (1998):

$$\mathrm{FF}(\alpha_{\mathrm{SIMS}}) = \frac{R_{\mathrm{SIMS}}}{R_{\mathrm{TRUE}}} \qquad (1)$$

where R_{SIMS} is the isotope ratio measured by SIMS and R_{TRUE} is the bulk value of the RM.

IMF was quantified using the equation:

$$\mathrm{IMF}\,(‰) = 1000\,(\alpha_{\mathrm{SIMS}} - 1) \qquad (2)$$

where α_{SIMS} is the fractionation factor from Equation 1.

TABLE 3. STABLE ISOTOPIC COMPOSITION OF THE SIX TOURMALINE RM

	δ^2H (‰)[1]	1SD (‰)	$\delta^{18}O$ (‰)[2]	1SD (‰)
BT01	–88	4	9.5	<0.1
BT02	–64	2	6.8	<0.1
DRG01	–47	2	13.4	<0.1
GE01	–50	6	19.7	<0.1
PE01	–105	2	12.3	<0.1
PE02	–83	4	10.8	<0.1

1: Measured by CF-IRMS
2: Measured by BrF5 method

TABLE 4. SIMS HOMOGENEITY TESTS OF TOURMALINE RM

	Hydrogen			Oxygen		
	no. grains	n	1SD (‰)	no. grains	n	1SD (‰)
BT01*	4	16	5	4	18	0.6
BT02	3	17	4	3	18	0.7
DRG01	3	11	4	3	12	1.0
GE01	3	11	4	3	12	0.8
PE01	3	11	4	3	12	0.8
PE02*	4	16	4	4	12	0.9

* Obtained from both calibration and oriented samples

The spot-to-spot repeatability was calculated for each grain analyzed. This is defined as the standard deviation of the IMF during a single SIMS session:

$$\text{Repeatability} = \sqrt{\frac{\sum \left(\text{IMF} - \text{IMF}_{\text{avg}}\right)^2}{(n-1)}} \qquad (3)$$

where IMF is the calculated instrumental mass fractionation for each spot (Eq. 2), IMF_{avg} is the average IMF for all analyses, and n is the total number of analyses.

Results

The tourmaline reference material in this study was evaluated for homogeneity with respect to elemental composition (electron probe microanalysis), bulk isotope composition (gas source mass spectrometry), and *in situ* isotope composition (secondary ion mass spectrometry).

Variation of the chemical composition of tourmaline RM is assessed by calculating the standard deviation for each element for several analytical spots on each grain. Major-element concentrations are consistent within each of the six tourmaline RMs (variation $\leq$0.40 wt.% for any individual element). Tourmalines were plotted by primary group based on *X*-site occupancy (Fig. 1a) and by species series based on *W*-site occupancy (Fig. 1b). The suite of RMs includes oxy- and fluor-tourmalines from the alkali and *X*-vacant groups (Fig. 1a, b). Tourmaline compo-

TABLE 5. HYDROGEN AND OXYGEN ISOTOPE DATA AS MEASURED BY SIMS

	June 10th, 2015						September 25th, 2020					
	n	$^2H/^1H_{SIMS}$	$^2H/^1H_{Bulk}$	FF[1]	IMF (‰)[2]	1SD (‰)[3]	n	$^2H/^1H_{SIMS}$	$^2H/^1H_{Bulk}$	FF[1]	IMF (‰)[2]	1SD (‰)[3]
BT01	6	0.0000537	0.0001421	0.3780	–622	3	5	0.0000522	0.0001421	0.3674	–633	5
BT02	6	0.0000479	0.0001458	0.3287	–671	3	8	0.0000467	0.0001458	0.3207	–679	5
DRG01	6	0.0000501	0.0001484	0.3372	–663	3	5	0.0000476	0.0001484	0.3207	–679	3
GE01	6	0.0000503	0.0001480	0.3400	–660	4	5	0.0000494	0.0001480	0.3337	–666	4
PE01	6	0.0000476	0.0001394	0.3418	–658	4	5	0.0000475	0.0001394	0.3404	–660	4
	March 21st, 2016						September 17th, 2020					
	n	$^{18}O/^{16}O_{SIMS}$	$^{18}O/^{16}O_{Bulk}$	FF[1]	IMF (‰)[2]	1SD (‰)[3]	n	$^{18}O/^{16}O_{SIMS}$	$^{18}O/^{16}O_{Bulk}$	FF[1]	IMF (‰)[2]	1SD (‰)[3]
BT01	3	0.0019239	0.0020242	0.9504	–49.6	0.7	5	0.0019393	0.0020242	0.9581	–41.9	0.7
BT02	3	0.0019138	0.0020188	0.9480	–52.0	0.7	8	0.0019277	0.0020188	0.9549	–45.1	0.6
DRG01	3	0.0019166	0.0020321	0.9432	–56.8	1.0	5	0.0019306	0.0020321	0.9501	–49.9	1.0
GE01	3	0.0019228	0.0020447	0.9404	–59.6	1.0	5	0.0019308	0.0020447	0.9443	–55.7	0.5
PE01	-	-	-	-	-	-	5	0.0019146	0.0020299	0.9432	–56.8	0.6

1: Calculated using Equation 1
2: Calculated using Equation 2
3: Calculated using Equation 3

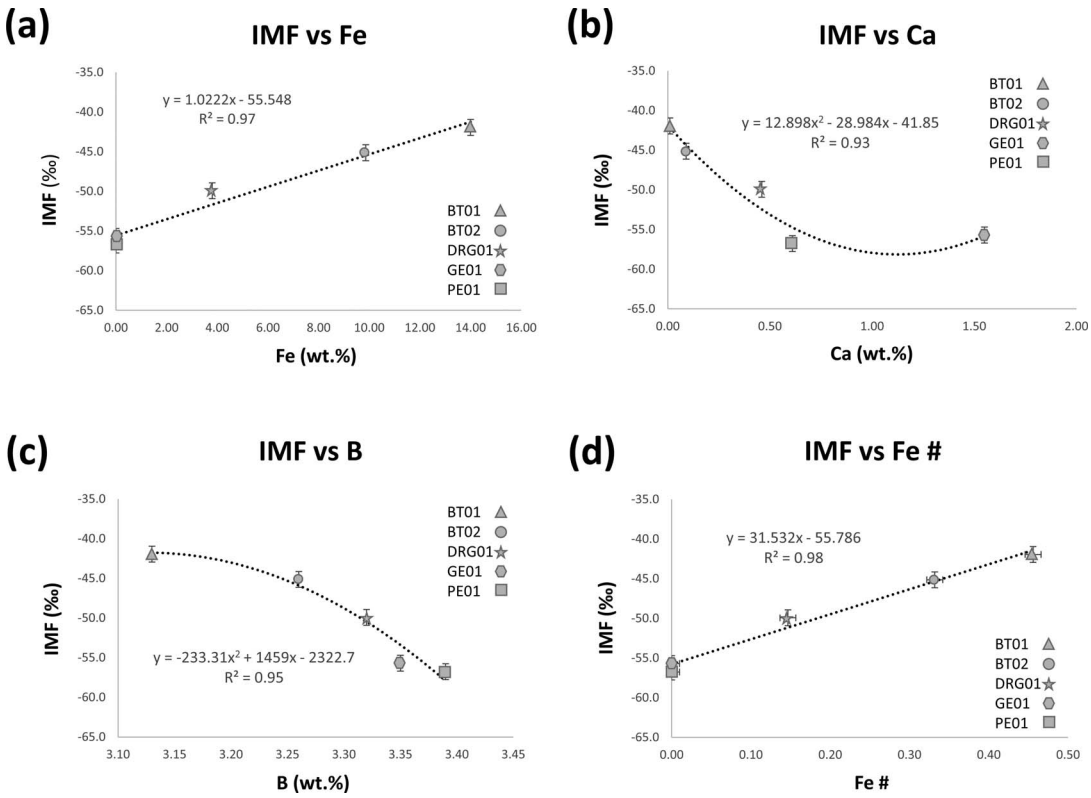

FIG. 3. Oxygen IMF (‰) *versus* (a) Fe, (b) Ca, (c) B, and (d) Fe#: Fe / (Fe + Mg + Al + Mn + Li) for the five tourmaline RM. The Fe and Fe# plots have a linear trend line, while the curves for Ca and B are defined by a 2nd order polynomial. Plots have an R^2 value of >0.93. Data is from the 2020 session; error bars not shown in the **x**-direction are collapsed into the size of the RM symbol.

sitions were plotted on the $2Li^{+}$–$^{Y}Fe^{2+}$–$^{Y}Mg^{2+}$ ternary (Fig. 1c) and as a function of ^{X}[□ / (□ + Na)] *versus* [Fe / (Fe + Li)] (Fig. 1d) and ^{X}[Ca / (Ca + Na)] *versus* ^{Y}[Fe / (Fe + Mg)] (Fig. 1e) and were named according to Henry *et al*. (2011: fluor-elbaite: PE01, PE02; fluor-dravite: GE01, DRG01; oxy-foitite: BT02; and fluor-schorl: BT01; Fig. 1c, d, and e, Table 2). The compositional variability of the RM suite is similar to that described in Marger *et al*. (2019; also plotted in Fig. 1) and is representative of the most common igneous and metamorphic tourmaline group minerals (*e.g*., schorl, elbaite, and dravite, see Fig. 2d, Marger *et al*. 2019).

Bulk hydrogen and oxygen isotope values for tourmaline RM are reported in Table 3. Hydrogen isotope values range from –105 to –47‰, with precision in the range 2–6‰ (1SD). Oxygen isotope values range from 6.8 to 19.7‰. Individual tourmaline grains (3–4 total) were also evaluated for *in situ* homogeneity for both hydrogen and oxygen isotope composition by SIMS (Table 4). Spot-to-spot repeatability (Eq. 3) was in the range 4–5‰ (1SD) and 0.6–1.0‰ (1SD) for hydrogen and oxygen isotopes, respectively.

Reference materials used to develop calibration curves (BT01, BT02, DRG01, GE01, and PE01) were analyzed for hydrogen and oxygen isotope ratios during four analytical sessions (Table 5). The IMF for hydrogen isotopes ratios for these samples ranged from –679 to –622‰. The IMF for oxygen isotope ratios ranged from –59.6 to –41.9‰. The average IMF for each calibration curve sample was plotted against the chemical composition of the tourmalines to investigate the relation between chemical composition and IMF. Furthermore, IMF was plotted *versus* the Fe# [(Fe / (Fe + Mg + Al + Ti + Mn + Li); *Y*-site occupants], which is commonly used for complex mineral systems (Ikert & Stern 2013, Śliwiński *et al*. 2016). Figures 2 and 3 show strong correlations (R^2 > 0.90) for both hydrogen and oxygen. For hydrogen, the strongest correlations with IMF are Fe ($R^2 = 0.95$), Si ($R^2 = 0.92$), B ($R^2 = 0.98$), and Fe# ($R^2 = 0.91$). For

TABLE 6. HYDROGEN AND OXYGEN ISOTOPE DATA AS MEASURED BY SIMS FOR ORIENTED SAMPLES

August 26th, 2015							
	n	$^{18}O/^{16}O_{SIMS}$	$^{18}O/^{16}O_{Bulk}$	FF[1]	IMF (‰)[2]	ΔIMF (‰)	1SD (‰)[3]
BT01-Cut1	5	0.0019194	0.0020242	0.9482	–51.8	0.8	0.5
BT01-Cut2	5	0.0019211	0.0020242	0.9490	–51.0	0.8	0.5
PE02-Cut1	5	0.0018919	0.0020269	0.9334	–66.6	0.2	0.8
PE02-Cut2	5	0.0018923	0.0020269	0.9336	–66.4	0.2	1.0
December 3rd, 2015							
	n	$^{2}H/^{1}H_{SIMS}$	$^{2}H/^{1}H_{Bulk}$	FF[1]	IMF (‰)[2]	ΔIMF (‰)	1SD (‰)[3]
BT01-Cut1	3	0.0000562	0.0001421	0.3958	–604	0	3
BT01-Cut2	3	0.0000562	0.0001421	0.3955	–604	0	5
PE02-Cut1	3	0.0000512	0.0001428	0.3583	–642	6	5
PE02-Cut2	3	0.0000520	0.0001428	0.3639	–636	6	3
September 25th, 2020							
	n	$^{2}H/^{1}H_{SIMS}$	$^{2}H/^{1}H_{Bulk}$	FF[1]	IMF (‰)[2]	ΔIMF (‰)	1SD (‰)[3]
BT01-Cut1	5	0.0000518	0.0001421	0.3647	–635	3	5
BT01-Cut2	5	0.0000522	0.0001421	0.3674	–633	3	5
PE02-Cut1	5	0.0000484	0.0001428	0.3392	–661	4	3
PE02-Cut2	5	0.0000490	0.0001428	0.3433	–657	4	3

Cut 1 is parallel to the **c**-axis
Cut 2 is perpendicular to the **c**-axis
1: Calculated using Equation 1
2: Calculated using Equation 2
3: Calculated using Equation 3
ΔIMF: Difference in instrumental mass fractionation between cuts 1 & 2

oxygen, the strongest correlations with IMF are Fe ($R^2 = 0.97$), Ca ($R^2 = 0.93$), B ($R^2 = 0.95$), and Fe# ($R^2 = 0.98$). A second-order polynomial best defines the curves produced for hydrogen isotope analysis with respect to Fe, Si, B, and Fe# (Fig. 2). For oxygen isotope analysis, there is a linear correlation between IMF and both Fe and Fe# (Fig. 3a and d), whereas a second-order polynomial best fits the curves for Ca and B (Fig. 3b and c).

The hydrogen and oxygen isotope compositions of two oriented RMs (PE02 and BT02) were analyzed during three sessions to test the influence of grain orientation on IMF when analyzed by SIMS (Table 6). The difference between the two orientations, defined as the difference between a grain mounted parallel and a grain mounted perpendicular to the **c**-axis (ΔIMF), for PE02 was 4–6‰ and 0.2‰, and for BT01 was 0–3‰ and 0.8‰, for hydrogen and oxygen isotope values, respectively.

Discussion

Calibration curves are commonly used to correct for IMF during SIMS analysis of minerals (Othmane *et al*. 2015, Marger *et al*. 2019). Often, this fractionation is related to a single element or a combination of elements. In this study, several elements correlate strongly with IMF and could be used to calibrate SIMS data (Fig. 2 and 3). However, we suggest that Fe is the best element to calibrate SIMS data for the following reasons.

First, within the tourmaline supergroup, Fe has a wider range in concentration than the other elements that strongly correlate to IMF. The total range of Fe content in the RM is 14.00 wt.% *versus* <2 wt.% for Si, B, and Ca. Thus, the use of Fe content may reduce error when calculating a correction factor for unknown samples. The chemical variability of the sample and uncertainties in the measurement of elemental composition are distributed over a wider compositional range, lessening the effects of this variation on an IMF *versus* element concentration curve fit.

Second, both δ^2H and $\delta^{18}O$ correlate strongly with B concentration. However, B is a difficult element to measure accurately *in situ* and requires advanced analytical techniques (*e.g*., SIMS, MC-LA-ICP-MS). Therefore, B content is often calculated using specialized software (*e.g*., WinTcac) that makes

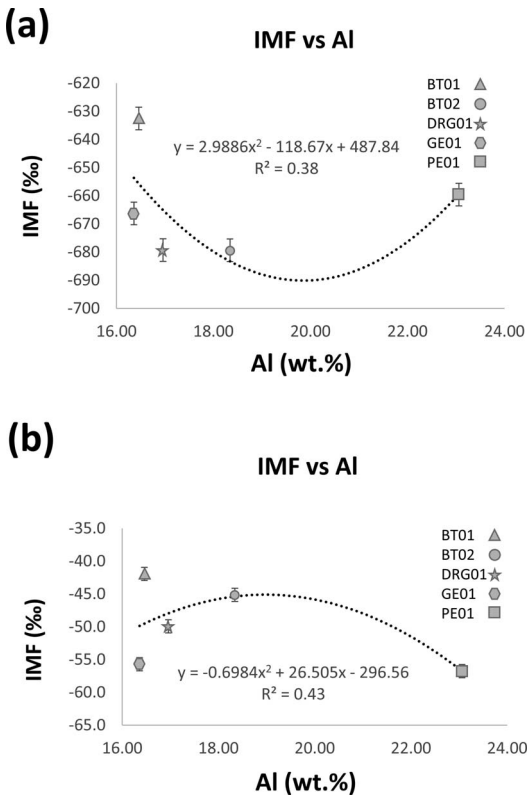

FIG. 4. Calculated IMF (‰) for (a) hydrogen and (b) oxygen *versus* Al for the five tourmaline RM. There is a very weak correlation between IMF and Al content for both plots; when fitted with a 2nd order polynomial curve the R^2 values are <0.44. Data is from the 2020 session; error bars not shown in the **x**-direction are collapsed into the size of the RM symbol.

several assumptions (*e.g.*, stoichiometric B_2O_3, B = 3 *apfu*) which may compound uncertainties (see Henry *et al*. 2011). The use of Fe avoids these complexities.

Finally, several studies have shown that the Fe content of a mineral is often the major contributor to IMF during isotope measurement by SIMS (Ikert & Stern 2013, Śliwiński *et al*. 2016, Marger *et al*. 2019). Our strong correlations for both the Fe and Fe# plots indicate that this is also the case for both hydrogen and oxygen isotopes in tourmaline. For oxygen isotopes, the trend line produced for Fe and Fe# is linear (Fig. 3a and d), whereas the Ca and B plots produce a second-order polynomial trend (Fig. 3b and c). A linear trend line can be fitted with greater confidence, and using fewer RMs, than a second-order polynomial fit.

For the above reasons, Fe content provides the most robust correction for hydrogen and oxygen isotope fraction in tourmaline as measured by SIMS. To the best of our knowledge, we report the first calibration curve used to correct for the fractionation of hydrogen isotope ratios. The following equations (Figs. 2a and 3a) define calibration curves using our analytical setup for hydrogen and oxygen isotope ratios with respect to Fe (wt.%):

$$\mathrm{IMF_{Hydrogen}} = 0.7768(\mathrm{Fe})^2 - 8.9389(\mathrm{Fe}) - 661.76 \quad (4)$$

$$\mathrm{IMF_{Oxygen}} = 1.0222(\mathrm{Fe}) - 55.548 \quad (5)$$

where IMF is the instrumental mass fractionation calculated for a single analysis of an unknown and Fe is the iron content (wt.%) of the unknown.

Marger *et al*. (2019) evaluated IMF during the analysis of oxygen isotopes in tourmalines on a large radius multi-collector SIMS instrument using mass-resolving power to resolve interferences. They observed a linear relation between IMF and the Fe and Al content of their tourmalines, with IMF varying by ~2.0 and 0.6‰, respectively. They reported a calibration scheme combining Fe and Al compositions in a weighted least squares regression. In our study, analysis was done on a small radius single-collector instrument using extreme energy filtering (EEF) to resolve interferences (Hervig *et al*. 1992). Our results also show that a linear relationship between IMF and Fe content of tourmalines exists (Fig. 3a). However, our results suggest that Al (wt.%) content of tourmaline does not correlate strongly with IMF for both H and O (Fig. 4a and b). Since Al (wt.%) content is not meaningfully related to IMF, the inclusion of this element in a regression with Fe would not improve the quality of our calibration curves (Fig. 4). Compared to the RM in the Marger *et al*. (2019) study, there is a clear absence of hydroxy-species tourmalines in the current study (Fig. 1b). The addition of these to our curves would allow a greater understanding of the isotope systematics during measurement by SIMS and could be the topic of future work.

Previous studies have shown that orientation effects must be considered during SIMS analysis of minerals, including rutile (Taylor *et al*. 2012), magnetite (Lyon *et al*. 1998), sphalerite, galena (Kita *et al*. 2011), and baddeleyite (Wingate & Compston 2000). When these minerals are mounted in different crystallographic orientations, they produce different secondary ionization yields. This effect has been credited to differential ionization of secondary species resulting from preferred channeling and focusing directions within the crystal structure (Kita *et al*. 2011) and emission of secondary ions along preferred structural directions (Wingate & Compston 2000). Marger *et al*. measured

oxygen (2019) and boron (2020) isotopes in oriented tourmaline samples and did not observe orientation effects. In our study, we analyzed two tourmalines (PE02 and BT01) mounted both parallel and perpendicular to the **c**-axis. The differences in IMF for both hydrogen and oxygen, for the two orientations, are within analytical uncertainty (Table 6). Therefore, orientation effects need not be considered for hydrogen and oxygen isotope analysis of tourmaline by SIMS.

Conclusions

We have developed calibration curves to correct hydrogen and oxygen isotope fractionation in tourmaline during SIMS analysis under extreme energy filtering conditions. We report the first calibration curve used to correct for the fractionation of hydrogen isotopes. Our results suggest that Fe content in tourmaline is strongly correlated to IMF. In fact, Fe provides the most robust correction for both hydrogen and oxygen isotope fractionation when a minimum of three RM (including those with both higher and lower Fe content than the unknowns) are used to accurately correct for matrix effects and IMF. Crystallographic orientation effects were not observed for our tourmalines.

Acknowledgments

This work was partially funded by an NSERC Discovery Grant to Mostafa Fayek and an NSERC Discovery Grant to FCH. The comments of Dr. Richard Stern and an anonymous reviewer greatly benefited the manuscript.

References

Adams, F., Micheiels, F., Moens, M., & Van Epsen, P. (1989) Secondary-ion mass spectrometry as a quantitative microanalytical technique. *Analytica Chimica Acta* **216**, 25–55. DOI: 10.1016/S0003-2670(00)82003-6

Clayton, R.N. & Mayeda, T.K. (1963) The use of bromine pentafluoride in the extraction of oxygen from oxides and silicate for isotopic analyses. G*eochimica et Cosmochimica Acta* **27**, 43–52. DOI: 10.1016/0016-7037(63)90071-1

Hawthorne, F.C. & Dirlam, D.M. (2011) Tourmaline the indicator mineral: From atomic arrangement to Viking navigation. *Elements* **7**, 307–312.

Henry, D.J. & Dutrow, B.L. (1996) Metamorphic tourmaline and its petrologic applications. *In* Boron: Mineralogy, Petrology, and Geochemistry (E.S. Grew & L.M. Anovitz, eds.). *Reviews in Mineralogy* **33**, 503–557.

Henry, D.J., Novák, M., Hawthorne, F.C., Ertl, A., Dutrow, B.L., Uher, P., & Pezzotta, F. (2011) Nomenclature of the tourmaline-supergroup minerals. *American Mineralogist* **96**, 895–913. DOI: 10.2138/am.2011.3636

Hervig, R.L., Williams, P., Thomas, R.M., Schauer, S.N., & Steele, I.M. (1992) Microanalysis of oxygen isotopes in insulators by secondary ion mass spectrometry. *International Journal of Mass Spectrom*etry **120**, 45–63. DOI: 10.1016/01681176(92)80051-2

Huberty, J.M., Kita, N.T., Kozdon, R., Heck, P.R., Fournelle, J., Spicuzza, M.J., Xu, H., & Valley, J.W. (2010) Crystal orientation effects of $\delta^{18}O$ for magnetite and hematite by SIMS. *Chemical Geology* **276**, 269–283. DOI: 10.1016/j.chemgeo.2010.06.012

Ickert, R.B. & Stern, R.A. (2013) Matrix corrections and error analysis in high-precision SIMS $^{18}O/^{16}O$ measurements of Ca–Mg–Fe garnet. *Geostandards and Geoanalytical Research* **37**, 429–448. DOI: 10.1111/j.1751-908X.2013.00222.x

Kita, N.T., Ushikubo, T., Fu, B., & Valley, J.W. (2009) High precision SIMS oxygen isotope analysis and the effect of sample topography. *Chemical Geology* **264**, 43–57. DOI: 10.1016/j.chemgeo.2009.02.012

Kita, N.T., Huberty, J.M., Kozdon, R., Beard, J.L., & Valley, J.W. (2011) High-precision SIMS oxygen, sulfur and iron stable isotope analyses of geological materials: Accuracy, surface topography and crystal orientation. *Surface and Interface Analysis* **43**, 427–431. DOI: 10.1002/sia.3424.

Kotzer, T.G. & Kyser, T.K. (1995) Petrogenesis of the Proterozoic Athabasca Basin, northern Saskatchewan, Canada, and its relation to diagenesis, hydrothermal uranium mineralization and paleohydrology. *Chemical Geology* **120**, 45–89. DOI: 10.1016/0009-2541(94)00114-N

Kozdon, R., Kita, N.T., Huberty, J.M., Foumelle, J.H., Johnson, C.A., & Valley, J.W. (2010) *In situ* sulfur isotope analysis of sulfide minerals by SIMS: Precision and accuracy, with application to thermometry of ~3.5 Ga Pilbara cherts. *Chemical Geology* **275**, 243–253. DOI: 10.1016/j.chemgeo.2010.05.015

Liu, R., Hull, S., & Fayek, M. (2011) A new approach to measuring D/H ratios with the CAMECA IMS-7F. *Surface and Interface Anal*ysis **43**, 458–461. DOI: 10.1002/sia.3467

Lyon, I.C., Saxton, J.M., & Turner, G. (1994) Isotopic fractionation in secondary ionization mass spectrometry. *Rapid Communications in Mass Spectrometry* **8**, 837–843. DOI: 10.1002/rcm.1290081009

Lyon, I.C., Saxton, J.M., & Cornah, S.J. (1998) Isotopic fractionation during secondary ionization mass spectrometry: Crystallographic orientation effects in magnetite. *International Journal of Mass Spectrometry and Ion Processes* **172**, 115–122. DOI: 10.1016/S0168-1176(97)00143-2

Marger, K., Luisier, C., Baumgartner, L.P., Putlitz, B., Dutrow, B.L., Bouvier, A.S., & Dini, A. (2019) Origin of

Monte Rosa whiteschist from in-situ tourmaline and quartz oxygen isotope analysis by SIMS using new tourmaline reference materials. *American Mineralogist* **104**, 1503–1520. DOI: 10.2138/am-2019-7012

Marger, K., Harlaux, M., Rielli, A., Baumgartner, L.P., Dini, A., Dutrow, B.L., & Bouvier, A. (2020) Development and re-evaluation of tourmaline reference materials for in situ measurement of boron δ values by secondary ion mass spectrometry. *Geostandards and Geoanalytical Research* **44**, 593–615. DOI: 10.1111/ggr.12326

Othmane, G., Hull, S., Fayek, M., Rouxel, O., Geagea, M.L., & Kyser, T.K. (2015) Hydrogen and copper isotope analysis of turquoise by SIMS: Calibration and matrix effects. *Chemical Geology* **395**, 41–49. DOI: 10.2138/am-2019-7012

Pouchou, J.L. & Pichoir, F. (1985) 'PAP' (φρZ) procedure for improved quantitative 513 microanalysis. *In* Microbeam Analysis (J.T. Armstrong, ed.). San Francisco Press, San Francisco, CA, USA (104–106).

Reid, K.D., Ansdell, K., Jiricka, D., Witt, G., & Card, C. (2013) Regional setting, geology, and paragenesis of the centennial unconformity-related uranium deposit, Athabasca Basin, Saskatchewan, Canada. *Economic Geology* **109**, 539–566. DOI: 10.2113/econgeo.109.3.539

Riciputi, L.R., Paterson, B.A., & Ripperdan, L.R. (1998) Measurement of light stable isotope ratios by SIMS: Matrix effects for oxygen, carbon, and sulfur isotopes in minerals. *International Journal of Mass Spectrom*etry **178**, 81–112. DOI: 10.1016/S13873806(98)14088-5

Shimizu, N. & Hart, S.R. (1982) Applications of the ion-microprobe to geochemistry and cosmochemistry. *Annual Review in Earth and Planetary Science* **10**, 483–526. DOI: 10.1146/annurev.ea.10.050182.002411

Shroeer, J.M., Rhodin, T.N., & Bradley, R.C. (1973) A quantum-mechanical model for the ionization and excitation of atoms during sputtering. *Surface Science* **34**, 571–580. DOI: 10.1016/0039-6028(73)90026-5

Sigmund, P. (1969) Theory of sputtering. I. Sputtering yield of amorphous and polycrystalline targets. *Physical Review* **184**, 386. DOI: 10.1103/PhysRev.184.383

Śliwiński, M.G., Kitajima, K., Kozdon, R., Spicuzza, M.J., Fournelle, J.H., Denny, A., & Valley, J.W. (2016) Secondary ion mass spectrometry bias on isotope ratios in dolomite–ankerite, Part I: δ18O Matrix effects. *Geostandards and Geoanalytical Research* **40**, 157–172. DOI: 10.1111/j.1751-908X.2015.00380.x

Taylor, R., Clark, C., & Reddy, S.M. (2012) The effect of grain orientation on secondary ion mass spectrometry (SIMS) analysis of rutile. *Chemical Geology* **300**, 81–87. DOI: 10.1016/j.chemgeo.2012.01.013

Valley, J.W. (2001) Stable isotope thermometry at high temperatures. *In* Stable Isotope Geochemistry (J.W. Valley and D.R. Cole, eds.). *Reviews in Mineralogy and Geochemistry* **43**, 365–413.

Wingate, M.T.D. & Compston, W. (2000) Crystal orientation effects during ion microprobe U-Pb analysis of baddeleyite. *Chemical Geology* **168**, 75–97. DOI: 10.1016/S00092541(00)00184-4

Yavuz, F., Karakaya, N., Yildirim, D.K., Karakaya, M.C., & Kumral, M.A. (2014) Windows program for calculation and classification of tourmaline-supergroup (IMA2011). *Computers and Geosciences* **63**, 70–87. DOI: 10.1016/j.cageo.2013.10.012

Received January 26, 2022. Revised manuscript accepted May 24, 2022.

This manuscript was handled by Associate Editor Jan Cempírek and Editors Lee Groat and Stephen Prevec.